

DOI: 10.17148/IJIREEICE.2025.131012

# Fuzzy Logic-Based Dual Phase-Shift PWM Strategy for Efficient Bidirectional Wireless Power Transfer in Electric Vehicles

## Mutta Murali Tarun<sup>1</sup>, P.Murari<sup>2</sup>

PG Student, Department of Electrical Engineering, Sankethika Vidya Parishad Engineering College, Andhra Pradesh, India<sup>1</sup>

HOD, Department of Electrical Engineering, Sankethika Vidya Parishad Engineering College, Andhra Pradesh, India<sup>2</sup>

**Abstract:** Bidirectional Wireless Power Transfer (BWPT) removes the need for physical intervention to facilitate smooth Grid-to-Vehicle (G2V) and Vehicle-to-Grid (V2G) operations; nevertheless, it still has drawbacks, including efficiency issues, power factor management, and low transfer rates. In order to enhance Power Factor Correction (PFC) in BWPT systems, this study suggests a Dual Phase Shift Pulse Width Modulation (DPS-PWM) technique. To improve the dynamic reaction and optimise switching choices in real-time depending on input changes and system behaviour, a Fuzzy Logic Controller (FLC) is also incorporated.

Simulation and experimental setups running at 85 kHz and 3.7 kW are used to assess the suggested intelligent control approach. The BWPT system is modelled and simulated using MATLAB/Simulink, which enables thorough performance study under various operating circumstances. The results show significant gains in Total Harmonic Distortion (THD) and overall system robustness, with a power transfer efficiency of 90.1% in the experiment and 94.4% in the simulation. Fuzzy logic integration has great promise for effective and adaptive control in next-generation BWPT systems for electric cars.

## I. OVERVIEW

The automobile industry has been greatly impacted by the growing concern over environmental sustainability and the depletion of fossil fuels, which has accelerated research and development in the electric vehicle (EV) sector [1]. The effectiveness and convenience of charging is one of the biggest obstacles preventing EVs from being widely adopted. Long recharge durations, safety hazards, and the requirement for human involvement are the main issues. Contactless energy transfer from a power source to a load is made possible via Wireless Power Transfer (WPT) technology, which presents a promising solution. When compared to traditional cable charging techniques, WPT improves user convenience and safety [2]. In addition to making charging easier, this technology lowers the hazards involved with physical connections by doing away with the need for charging cords. Additionally, human-free charging enables smaller and lighter battery designs, shorter charging times, and the freedom to charge devices anywhere there is a compatible outlet [3]. In addition to EVs, WPT is being used in a number of high-power and specialised applications, including underwater vehicles, train traction systems, and wirelessly powering medical implants [4], [5]. These uses highlight WPT's wider potential to address battery-powered devices' drawbacks, namely as short battery life and expensive initial prices. WPT is becoming more and more popular because of its qualities, which include high reliability, user ease, operational safety, and resilience to environmental conditions [6]. Particularly, developing technologies that rely on bidirectional energy transfer, such as Vehicle-to-Home (V2H), Vehicle-to-Vehicle (V2V), and Vehicle-to-Grid (V2G), are made possible by Bidirectional Wireless Power Transfer (BWPT). For high-frequency operation across primary and secondary bridges, modern BWPT systems include completely regulated switching components such SiC MOSFETs and IGBTs. A common block diagram showing the integration of photovoltaic (PV) systems, wirelessly connected electric vehicles (EVs), a DC bus, and the power grid in V2G and G2V scenarios is shown in Figure 1. EVs help to improve grid stability and power quality by taking part in active and reactive power management [7]. Power factor and Total Harmonic Distortion (THD) must be kept within reasonable bounds in grid-connected systems. In wireless charging systems, power electronic converters are essential for maintaining power quality. However, the Wireless Power Transfer (WPT) system may not work as well as it should due to a number of variables, including coil misalignment, parameter detuning, coil distance fluctuations, and load volatility [9]. These variations may result in higher power losses, less effective power transmission, difficulties with soft switching, and increased component stress. To guarantee the seamless integration of Bidirectional Wireless Power Transfer (BWPT) systems with the power grid, it is especially important to maintain a high power factor.



DOI: 10.17148/IJIREEICE.2025.131012

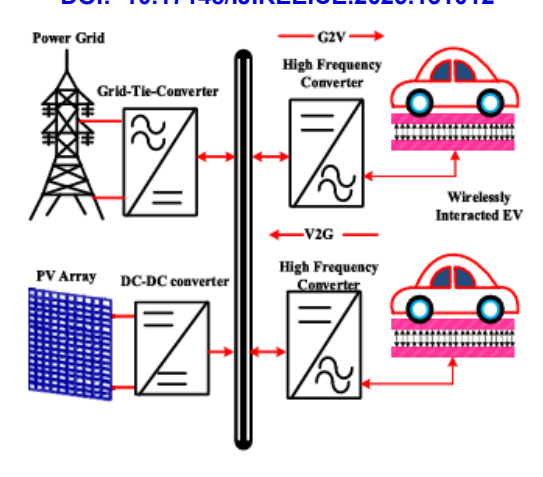


FIGURE 1(a). An example of EVs that are wirelessly connected in the V2G and G2V services.

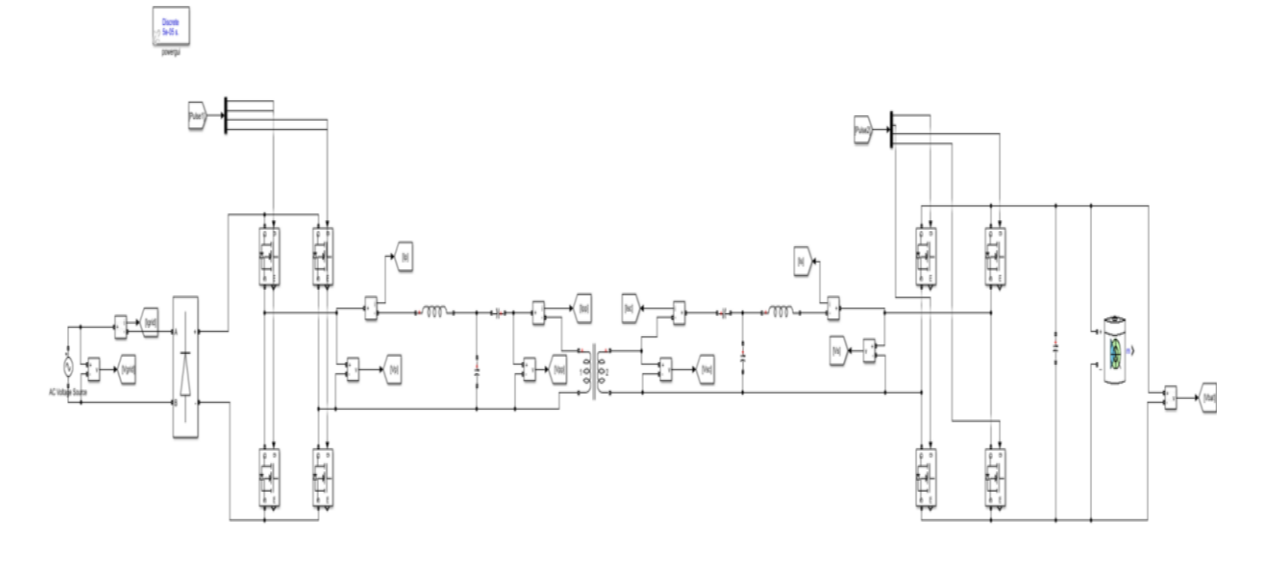


FIGURE1(b). V2G and G2V circuit diagram

## II. WPT SYSTEM BIDIRECTIONAL

In a Bidirectional Wireless Power Transfer (BWPT) system, Electric Vehicles (EVs) connect to the DC bus through a wireless charging mechanism. Each component of the system is meticulously designed, featuring coupling coils, highfrequency power converters, compensation circuits, and intelligent control units. The schematic representations of the proposed system in both charging (G2V) and discharging (V2G) modes are depicted in Figures 2 and 3. In Grid-to-Vehicle (G2V) mode, the primary-side converter functions as a DC/AC inverter, delivering high-frequency power to the transmitting coil. At the same time, the secondary-side converter acts as a regulated AC/DC rectifier to charge the EV battery. In contrast, during Vehicle-to-Grid (V2G) mode, the direction of power flow is reversed—the EV battery serves as the power source, and the converters swap roles to supply power back to the grid [11]. The proposed circuit features an LCC-based resonant converter along with a full-bridge inverter on the primary side, complemented by a corresponding converter on the secondary side. Within this bidirectional fuzzy-controlled framework, the control strategy dynamically modifies the duty cycle of the inverters based on fuzzy logic rules that react to real-time voltage, current, and load conditions. By managing the average low-frequency components of the voltages at both ends (primary VPV PVP and secondary VSV SVS), the fuzzy controller guarantees stable and efficient power regulation. Both the primary and secondary sides are equipped with resonance compensation networks, which are essential for achieving high-efficiency energy transfer through mutual inductance. Under resonant conditions, energy is wirelessly transmitted from the primary coil to the secondary coil. In this context, the fuzzy logic controller continuously observes critical variables (such as coil alignment, load fluctuations, and coupling coefficient) and intelligently modifies inverter parameters to sustain optimal performance.



#### DOI: 10.17148/IJIREEICE.2025.131012

An advanced Pulse Width Modulation (PWM) technique is frequently utilized for phase shift control in Bidirectional Wireless Power Transfer (BWPT) systems. This method entails the generation of control signals for the converter switches on both the primary and secondary sides to effectively manage power flow. In conventional implementations, fundamental control strategies take into account the dual functionality of both converters—operating either as rectifiers or inverters—based on the direction of energy transfer. In Grid-to-Vehicle (G2V) mode, where the battery receives charge from the grid, the primary converter operates as a high-frequency inverter, while the secondary converter serves as a controlled rectifier. The phase difference between the voltage waveforms on both sides dictates the direction and magnitude of power flow. Nevertheless, sustaining optimal performance under varying conditions (such as load fluctuations, coil misalignment, and coupling variations) poses a significant challenge. To tackle these nonlinearities and uncertainties, a fuzzy logic-based control strategy is incorporated with the phase shift PWM control. The fuzzy controller adjusts the phase angle dynamically, based on real-time input parameters such as voltage error, power deviation, and load conditions. In contrast to classical controllers that necessitate precise models and fixed tuning, fuzzy logic is capable of managing imprecise data and facilitates adaptive decision-making through established fuzzy rules.

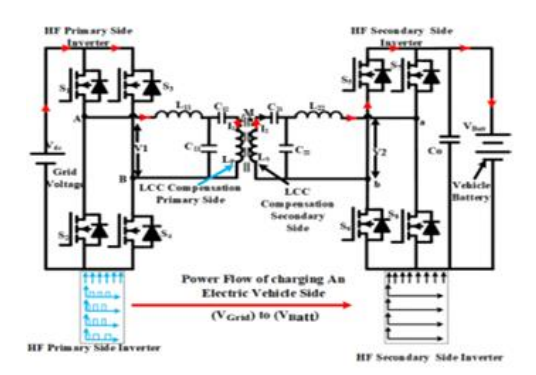


FIGURE 2. BWPT system for the Operation of (VGrid) Side to (VBatt) Side.

An advanced Pulse Width Modulation (PWM) technique is frequently utilized for phase shift control in Bidirectional Wireless Power Transfer (BWPT) systems. This method entails the generation of control signals for the converter switches on both the primary and secondary sides to effectively manage power flow. In conventional implementations, fundamental control strategies take into account the dual functionality of both converters—operating either as rectifiers or inverters—based on the direction of energy transfer. In Grid-to-Vehicle (G2V) mode, where the battery receives charge from the grid, the primary converter operates as a high-frequency inverter, while the secondary converter serves as a controlled rectifier. The phase difference between the voltage waveforms on both sides dictates the direction and magnitude of power flow. Nevertheless, sustaining optimal performance under varying conditions (such as load fluctuations, coil misalignment, and coupling variations) poses a significant challenge. To tackle these nonlinearities and uncertainties, a fuzzy logic-based control strategy is incorporated with the phase shift PWM control. The fuzzy controller adjusts the phase angle dynamically, based on real-time input parameters such as voltage error, power deviation, and load conditions. In contrast to classical controllers that necessitate precise models and fixed tuning, fuzzy logic is capable of managing imprecise data and facilitates adaptive decision-making through established fuzzy rules.

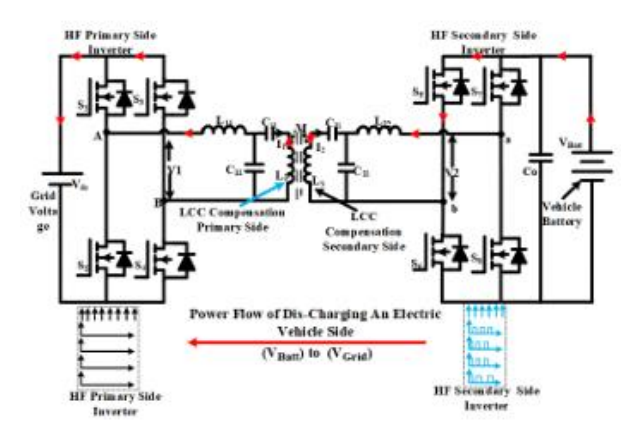


FIGURE 3. BWPT system for the Operation of (VBatt) Side to (VGrid) Side.



#### DOI: 10.17148/IJIREEICE.2025.131012

The primary-side converter is regulated through Phase Shift Modulation (PSM), while the secondary-side converter concurrently operates as a rectifier—enabling controlled AC to DC conversion during energy transfer. This synchronized operation is depicted in Figure 2, which illustrates the G2V (Grid-to-Vehicle) charging mode. In contrast, during V2G (Vehicle-to-Grid) discharging, as represented in Figure 3, the primary-side AC/DC converter functions as a rectifier, while the secondary-side DC/AC converter serves as an inverter—permitting the transfer of stored energy from the battery back to the grid. To efficiently manage active power flow and enhance real-time performance, a fuzzy logic-based coordination between the converters is implemented. This approach facilitates dynamic adjustments by continuously assessing system variables such as voltage error, current feedback, and load demand. Unlike fixed control schemes, fuzzy controllers exhibit greater tolerance to nonlinearities, allowing for soft decision-making even in uncertain conditions such as coil misalignment or parameter drift. For optimal operation, both converters must operate in harmony. This is accomplished through a wireless control link that diminishes reliance on conventional signal-processing pathways, thereby reducing latency and enhancing responsiveness. With this configuration, the converters remain synchronized, and the control strategy is both programmable and flexible, providing adaptive tuning for real-time system optimization and high efficiency in both charging and discharging modes.

## III. CONTROL OF PHASE SHIFT

The value of  $\alpha$ , which is established by the reference signal, is essential for the primary side circuit to function at the rated current of the secondary controller. It facilitates accurate adjustment of the output voltage of the primary side inverter. The secondary controller produces the phase shift ( $\beta$ ) between the legs of the secondary inverter, which affects the correlation between the output voltages on the primary and secondary sides. Low-level switching signals are utilized to execute the PWM technique, which are subsequently refined by fine-tuning the phase shift parameters ( $\alpha$ ,  $\beta$ , and  $\delta$ ) for both the left and right sides [16].

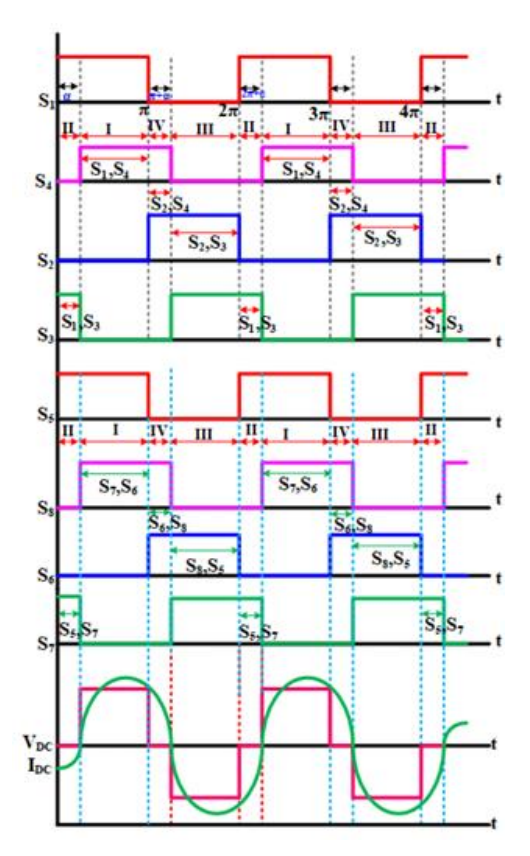


FIGURE 8. Switching waveforms of BWPT for V2G and G2V Operation.

To attain the desired magnitude and direction of power flow, the secondary control parameters ( $\beta$  and  $\delta$ ) must be modified. The configuration of the four switches on each side of the high-frequency converters is dictated by signals amplified by the driving circuits. These control parameters are vital in altering the amplitude and phase of the inverter voltages, thereby ensuring proper power flow throughout the system [17].



DOI: 10.17148/IJIREEICE.2025.131012

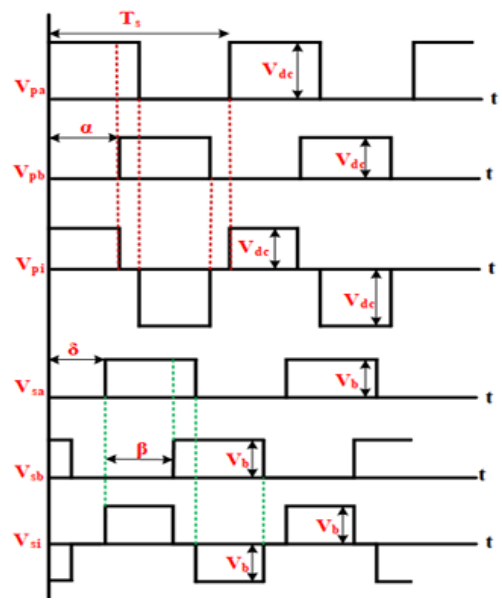


FIGURE9. Switching waveforms of phase angle delay between the two converters.

In a BWPT system, both sides can operate as both a load and a supply concurrently, necessitating equal treatment for all components. To guarantee that the full-bridge converters on the primary and secondary sides engage simultaneously, a deliberate delay in the activation of the semiconductor switches at both ends is required. The power flow between the primary and secondary converters (AC/DC and DC/AC) is regulated using phase angles ( $\alpha$ ,  $\beta$ ) and the delay angle ( $\delta$ ). The switching waveforms and the phase angle delay between the two converters are illustrated in Figure 9. Generally, the power level is modulated on both sides by adjusting the phase shift angle. The delay angle ( $\delta$ ) signifies the phase difference between the peak voltages of the primary and secondary inverters [18].

The output voltages for the first harmonics, VP(t) and VS(t), are written as

$$V_p(t) = \left(\frac{4}{\pi}\right) V_p \sum_{n=1,3}^{\infty} \frac{1}{n} \cos\left(n\omega_r t - \frac{n\alpha}{2}\right) \sin\left(\frac{n\alpha}{2}\right)$$
 (1)

$$V_p(t) = \left(\frac{4}{\pi}\right) V_p \sum_{n=1,3}^{\infty} \frac{1}{n} \cos\left(n\omega_r t - \frac{n\alpha}{2}\right) \sin\left(\frac{n\beta}{2}\right)$$
 (2)

In the equation presented above, the sequence of harmonics is indicated by "n." The variables  $\alpha$  and  $\beta$  signify the phase shift occurring between the switches of a pair of inverters, whereas VP and VS represent the peak voltages of the inverters on the primary and secondary sides, respectively. The term "n" pertains to the orders of harmonics.

## IV. THE BWPT SYSTEM DESIGN PARAMETERS

To create BWPT systems, it is essential to develop a phase shift controller that incorporates enhanced Power Factor Correction (PFC) control. This development guarantees efficient power transfer between the primary and secondary coils at the resonance frequency.

$$P=\omega 0MI p I s$$
 (3)

This example demonstrates the mutual inductance present between the primary and secondary coils. The variables IP and IS denote the Root-Mean-Square (RMS) currents that flow through the primary and secondary coils, respectively. The mutual inductance of these coils is vital for wireless charging systems, as it significantly influences the efficiency and effectiveness of power transfer. In this particular case, the operating frequency of 85 kHz adheres to the SAEJ2954

standard. Consequently, the formula for the output power is expressed as follows: 
$$p = 2\pi f \theta(N_p I_p)(N_s I_s) K \sqrt{\hat{L}_p \hat{L}_s}$$
(4)

The operating frequency is indicated as f0, with NP and NS signifying the number of turns in the primary and secondary coils, respectively. The inductance returns for the primary and secondary coils are denoted by ^LP and ^LS. K represents

International Journal of Innovative Research in Electrical, Electronics, Instrumentation and Control Engineering
Impact Factor 8.414 

Refereed journal 

Vol. 13, Issue 10, October 2025

#### DOI: 10.17148/IJIREEICE.2025.131012

the coupling coefficient between the coils, where a reduced air gap results in a higher K value, while an increased air gap leads to a lower K. These equations determine the mutual inductance per return based on the dimensions of the coils and the air gap separating the charging pads.

$$M = K\sqrt{L_p * L_s} \quad (5)$$

$$IP = \frac{V_{AB}}{\omega 0 L II}, I_S = \frac{V_{ab}}{\omega 0 L 22}$$
 (6)

$$V_{LP} = I_P X_{LP} = j\omega L_P I_P = I_P (2\pi N_p^2 \hat{L}_p)$$
 (7)

$$V_{Ls} = I_s X_{Ls} = j\omega L_s I_s = I_s \left(2\pi N_p^2 \hat{L}_p\right) \quad (8)$$

According to equation (6), the compensatory inductances L11 and L22 have an impact on the currents IP and IS, which subsequently affect the input-output voltage. A modification in the compensating inductance L11 facilitates a decrease in the coil current IP. Through LCC-LCC compensation, various ranges of coil current (IP) for a specific voltage can be established, and the number of turns (NP) can be specified [23]. Nevertheless, selecting an excessively high number of turns to diminish the coil's current leads to a considerable increase in the coil's inductance and voltage. This situation can result in extremely high voltages, which may introduce security and reliability concerns due to the insulating layer and the distance between turns of the Litz wire. Additionally, certain applications may impose restrictions on the maximum allowable system voltage. As a result, the voltage across the coils and capacitors constrains the number of turns, and equations (7) and (8) can be utilized to quantitatively characterize this relationship.

$$G_{Vp} = \frac{V_{LP}}{V_{AB}} = \frac{X_{LP}}{X_{LII}} = \frac{L_P}{LII}$$
 (9)

$$\omega_0 = \frac{I}{\sqrt{L_{II}C_{II}}} = \frac{I}{\sqrt{(L_P - LII)CI2}}$$
 (10)

$$\omega_{\theta} = \frac{1}{\sqrt{L_{2}C_{2}}} = \frac{1}{\sqrt{(L_{c} - L_{2}^{2})C_{2}^{2}}}$$
(11)

$$IL_{II} = \frac{MV_{AB}}{\omega_0 L_{II} L_{22}}, L_{22} = \frac{MV_{ab}}{\omega_0 L_{II} L_{22}}$$
 (12)

$$IL_{II} = \frac{MV_{AB}}{\omega 0L_{II}}, L_{LS} = \frac{V_{ab}}{\omega 0L_{22}}$$
 (13)

$$V_{C12} = \frac{V_{AB}(L_P - L_{II})}{LII} \tag{14}$$

$$V_{C21} = \frac{V_{AB}(L_S - L_{22})}{L_{22}} \tag{15}$$

Moreover, the high-frequency high-power capacitor is required to satisfy both the voltage and current specifications, while also considering the limitations imposed by heating. The actual rated voltages and currents for the resonant tank components of the proposed design are presented in Table 1.

## V. Correction of the Power Factor INTHEBWPTSYSTEM

S: No	Parameters	Symbols	Values
1	Output Power	$P_{out}$	3.7 kW
2	Input AC voltage	$V_{Grid}$	325 V
3	Output Converter Voltage	$V_{out}$	420 V
4	Coupling Co-efficient	K	0.4
5	Switching Frequency	$f_s$	85 kHz
6	Mutual Inductance	M	46.5µH
7	Capacitor for Primary Side Series Compensation	$C_p$	31nF
8	Self-Inductance of the Primary Coil	$L_P$	120 μΗ
9	Secondary Coil Self Inductance	$L_{\text{S}}$	120 μΗ
10	Secondary Side Series Compensation Capacitor	$C_{S}$	31nF
11	Capacitance Filter	$C_0$	30 μF

TABLE1. Electrical circuit parameters of 3.7 KW BWPT system.



International Journal of Innovative Research in Electrical, Electronics, Instrumentation and Control Engineering
Impact Factor 8.414 

Refereed journal 

Vol. 13, Issue 10, October 2025

DOI: 10.17148/IJIREEICE.2025.131012

$$P_o = \frac{8}{\pi^2} * \frac{V_P * V_S}{\omega * L_M} \tag{16}$$

Power Factor Correction (PFC) can be implemented either at the front-end or back-end of an ideal Wireless Power Transfer (WPT) system. Nevertheless, the choice between front-end and back-end PFC is influenced by various factors, such as system requirements, efficiency considerations, and design constraints [25]. Each method presents its own set of advantages and disadvantages, and the decision should be based on the specific requirements of the system. In an ideal WPT system,

$$P_a(t) = 2V_a I_a \sin(\omega_a t) \tag{17}$$

In this context, Vg and Ig denote the input voltage and RMS current of the grid, respectively.

Consequently, the power transfer can be computed as follows:

$$P_g(t) = V_g I_g = P_{mean}(1 + \cos(2\omega_g))$$
 (18)

This research posits that continuous current (CC) and continuous voltage (CV) control collaborate to manage the batteries. The readings of battery current and voltage will be utilized to operate this control system. To facilitate CC management, a current saturation mechanism has been introduced. The internal current control loop, which effectively mitigates both internal and external disturbances, is essential for ensuring precise current regulation. The transmitted power can be determined as follows, given that the secondary-side voltage and resonant current are consistently synchronized.

$$p = \frac{p_{mean}^* M \omega_0 \pi}{2 V_{BAT}} = \frac{4}{\pi \omega_0 i \hat{P}}$$
 (19)

$$v_{\widehat{Pf} = \frac{4}{\pi} V_r \sin(\delta_P \pi/2)} \tag{20}$$

$$v_{\widehat{Pf} = \frac{4}{\pi} V_{BAT} \sin(\delta_P \pi/2)} \tag{21}$$

The primary and secondary duty cycles are denoted by  $\delta p$  and  $\delta s$ , respectively. VBAT indicates the battery voltage, whereas Vr signifies the rectified grid voltage. Both PFC control strategies require a grid-connected 50 Hz active rectifier, irrespective of the converter employed for PFC and current shaping.

Resonant inverters manage the primary resonant tank (VP) and the current flow between the primary and secondary coils by modifying the unregulated AC voltage. Furthermore, when an off-board primary-side resonant inverter is responsible for power control, communication systems or estimation techniques become necessary.

## VI. OUTCOMES AND TALK

A simulation analysis and experimental verification have been carried out for the proposed system, which has a power rating of 3.7 kW, as outlined in Table 1. The MATLAB simulation encompasses both G2V and V2G operational modes. Key parameters, including grid-side voltage and current, transmitter and receiver coil sides, as well as inverter output, are recorded. The output voltage at the secondary inverter side (Vout) measures 420V, while the input AC voltage (VGrid) is 325V. These simulation parameters are consistent with the established guidelines. The system functions at a switching frequency (fs) of 85 kHz and a coupling coefficient (K) of 0.4. The system components consist of the primary coil's self-inductance (LP), the secondary coil's self-inductance (LS), the secondary side series compensation capacitor (CS), the capacitance filter (C0), and the primary side series compensation capacitor (CP). The mutual inductance (M) is estimated to be 46.5µH. This simulation study offers a thorough analysis of the performance of the proposed dual-phase shift Pulse Width Modulation (PWM) technique across various operating conditions.

## A. G2V SIDE SIMULATION RESULTS

Initially, the G2V operational simulation mode is employed, taking into account a grid frequency of 50 Hz and a grid supply voltage magnitude of 325V. The sinusoidal fluctuation of the nominal grid input voltages is illustrated in Figure 16(a).

International Journal of Innovative Research in Electrical, Electronics, Instrumentation and Control Engineering
Impact Factor 8.414 

Refereed journal 

Vol. 13, Issue 10, October 2025

DOI: 10.17148/IJIREEICE.2025.131012

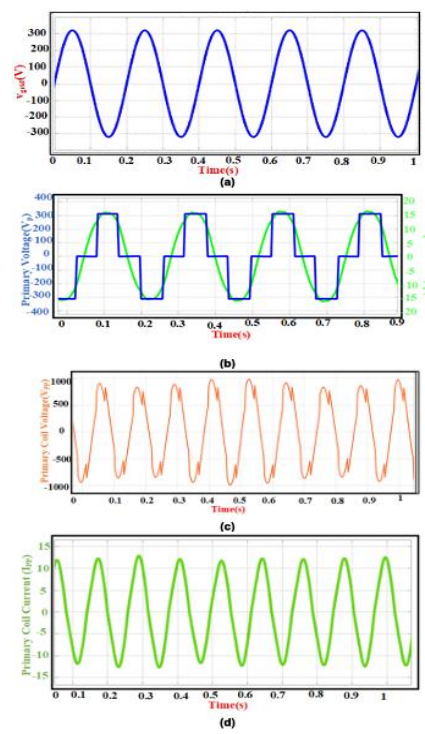


FIGURE 16. (a) The Grid Input Voltage (b) Primary side Converter voltage control (Vpp) Current (Ipp) (c) Primary coil voltage (Vpp) across the transmitter pads (Vpp) (d) The Primary coil current across the transmitter pads (Ipp).

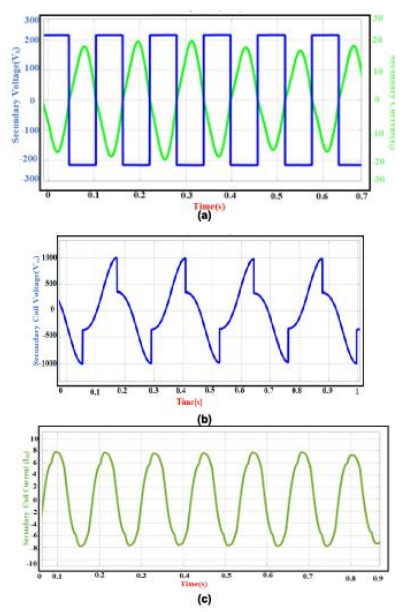


FIGURE 17. (a) Secondary side Converters voltage control (Vss) Current (Iss) Waveforms (b) Secondary coil voltage (Vss) across the Receiver pads (c) Secondary coil Current (Iss) across the Receiver pads.

The harmonic level at the coil's end is diminished by the compensating resonance capacitance present at the output of the secondary converter, which also contributes to a reduction in the Total Harmonic Distortion (THD). Simulation outcomes for G2V operation indicate that control on the primary side offers superior regulation of THD and bifurcation at both the primary and secondary ends. Conversely, the same Power Factor Correction (PFC) is attained during G2V operation via unregulated operation on the secondary side.



DOI: 10.17148/IJIREEICE.2025.131012

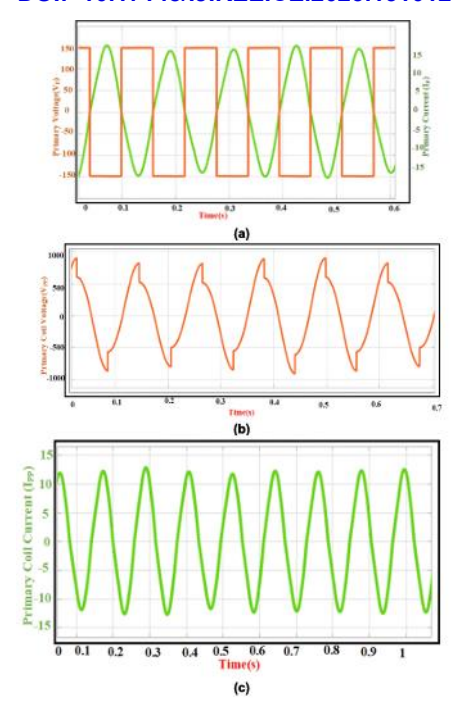


Fig. 18. Current (Ipp) at the primary side, converter voltage (Vpp), voltage (Vpp) across the primary pads, and primary coil current (Ipp) are the first three variables.

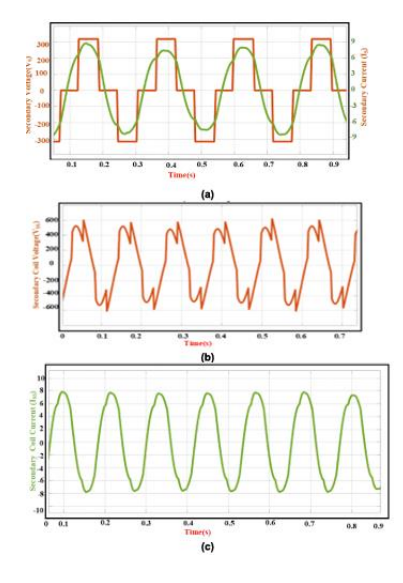


FIGURE 19. (a) Secondary side Converter voltage control (Vss) Current (Iss) (b) Secondary side coil voltage (Vss) across the Receiver Pads (c) Secondary side coil Current (Iss) across the Receiver Pad.

## **B. V2G SIDE SIMULATION RESULTS**

In the V2G segment of the simulation study, the secondary converter is regulated while the primary side converter is left unmodulated. Aside from the alterations in the control flow, the design parameters are consistent with those employed in the G2V operation. The voltage and current of the primary side unregulated square-wave modulation converter are illustrated in Figure 18(a).

## C. G2V OPERATION WITH FUZZY-ENHANCED CONTROL

The Grid-to-Vehicle (G2V) operational simulation mode initiates with a grid frequency of 50 Hz and a grid supply voltage magnitude of 325 V. The sinusoidal fluctuation of the nominal grid input voltage is illustrated in Figure 20(a). The voltage and current waveforms of the primary side converter operating under fuzzy control are represented in Figure 20(b), where

International Journal of Innovative Research in Electrical, Electronics, Instrumentation and Control Engineering
Impact Factor 8.414 

Refereed journal 

Vol. 13, Issue 10, October 2025

#### DOI: 10.17148/IJIREEICE.2025.131012

a notable decrease in Total Harmonic Distortion (THD) is evident when functioning in G2V mode with primary-side control. Nevertheless, Figures 20(c) and 20(d), which depict the voltage and current on the primary coil, underscore the existence of voltage harmonics within the system. In this configuration, the modulated current (Ipp) on the primary coil is approximately 12 A, accompanied by a modulated voltage (Vpp) of around 940 V.

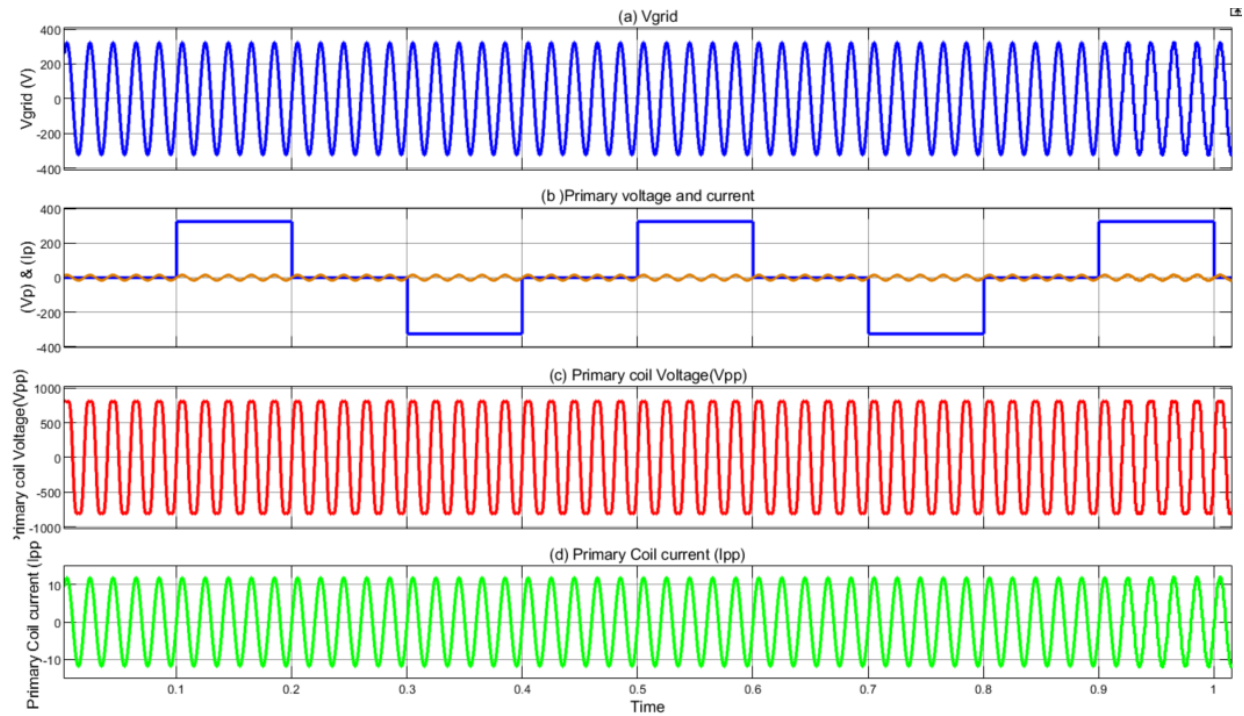


**FIGURE 20.** (a) Grid input voltage waveform (50 Hz, 325 V RMS) under fuzzy logic-based control. (b) Primary-side converter voltage (Vpp) and current (Ipp) with fuzzy-optimized dual-phase PWM, showing reduced THD. (c) Primary coil voltage (Vpp) across transmitter pads with improved harmonic suppression due to fuzzy control.(d) Primary coil current (Ipp) under fuzzy logic control, highlighting stable waveform and enhanced power factor.

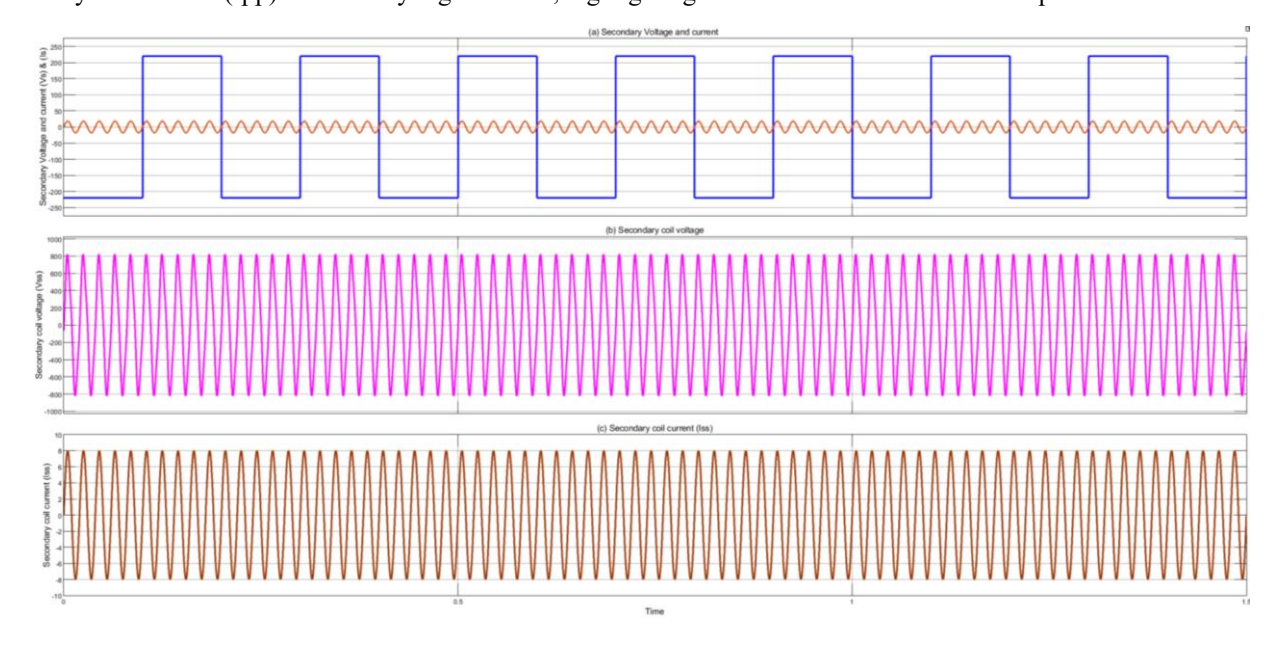


**FIGURE 21.**(a) Secondary-side converter voltage (Vss) and current (Iss) waveforms under unregulated control, with fuzzy logic-based system monitoring. (b) Secondary coil voltage (Vss) across receiver pads, showing voltage harmonics. (c) Secondary coil current (Iss) across receiver pads, with fuzzy logic aiding in THD reduction via adaptive resonance compensation.

International Journal of Innovative Research in Electrical, Electronics, Instrumentation and Control Engineering
Impact Factor 8.414 

Refereed journal 

Vol. 13, Issue 10, October 2025



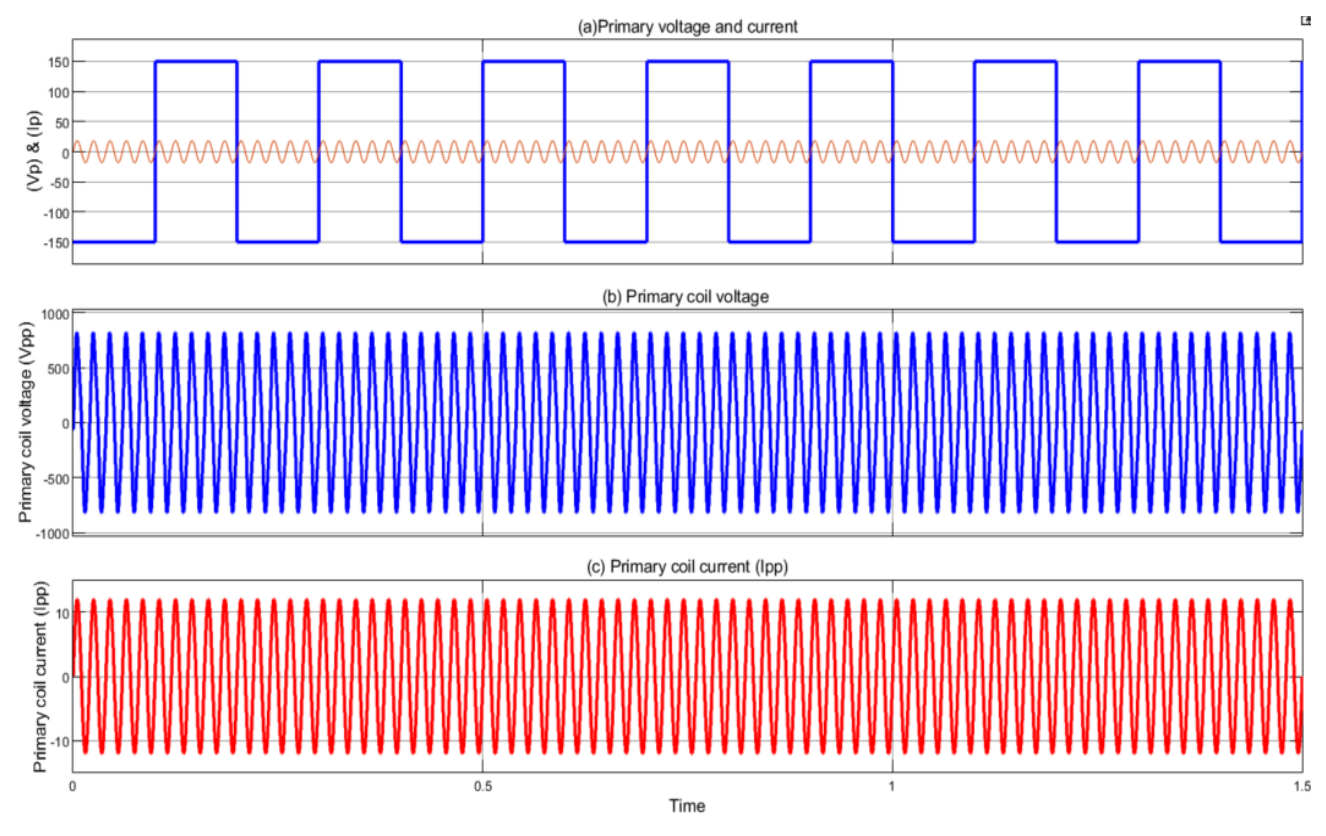


FIGURE 22. (a) Primary-side unregulated converter voltage (Vpp) and current (Ipp) under square-wave modulation in V2G mode. (b) Voltage (Vpp) across primary transmission pads. (c) Primary coil current (Ipp) under fuzzy logic-monitored secondary-side control, showing reduced THD in current.

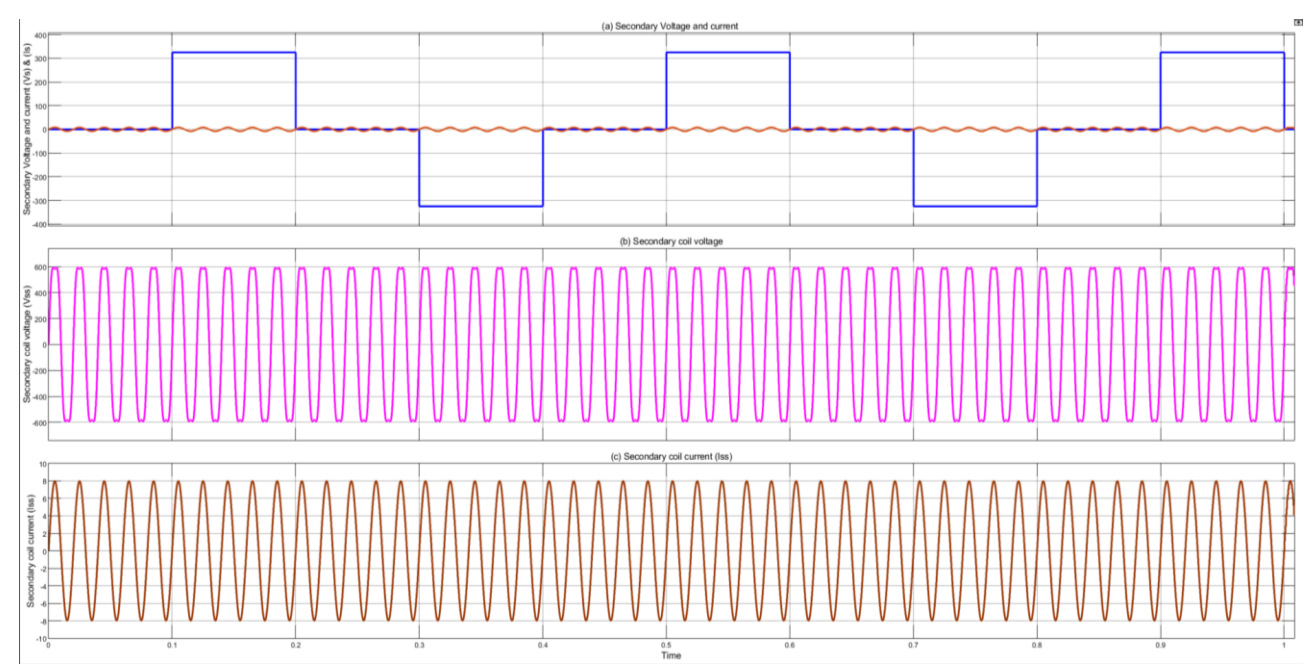


FIGURE 23. (a) Secondary-side converter voltage (Vss) and current (Iss) under fuzzy logic-optimized V2G control. (b) Secondary coil voltage (Vss) across receiver pads. (c) Secondary coil current (Iss), with fuzzy logic ensuring waveform stability and improved PFC



DOI: 10.17148/IJIREEICE.2025.131012

## D. V2G OPERATION WITH FUZZY LOGIC-ENHANCED CONTROL

During the Vehicle-to-Grid (V2G) operation, the control responsibility transitions to the secondary converter, while the primary side converter functions in an unmodulated square-wave mode. The design parameters remain aligned with those utilized in the Grid-to-Vehicle (G2V) mode, with the exception of the alteration in the control strategy. In Figure 22(a), the primary side voltage (Vpp) and current (Ipp) waveforms are illustrated under unregulated operation, showcasing peak values of 150 V and 10 A, respectively. Figures 22(b) and 22(c) depict the voltage and current waveforms across the primary pad, where it is apparent that the current waveform displays a more sinusoidal shape in comparison to the voltage. The Total Harmonic Distortion (THD) of the current is significantly lower than that of the voltage, indicating the natural smoothing effect resulting from inductive coupling.

The incorporation of an Artificial Neural Network (ANN) enhances the system's capability to track signals in real-time and make predictive adjustments on the secondary side. Consequently, even with control emanating from the secondary converter, the system enhances Power Factor Correction (PFC) on the primary side. The ANN dynamically adapts to varying load and grid conditions, ensuring stable power flow, improved converter synchronization, and minimized control delays. On the secondary side, Figure 23(a) illustrates the converter voltage and current with amplitudes of 310 V and 8 A, respectively. The voltage and current waveforms on the secondary coil, as shown in Figures 23(b) and 23(c), reach 600 V and 8 A. The ANN-based control optimizes the modulation of the secondary side, guaranteeing stable operation while effectively managing voltage harmonics. While bifurcation and THD do not exhibit significant changes in V2G mode, the ANN-enhanced control contributes to a more consistent PFC, alleviates transient instability, and ensures efficient bidirectional energy exchange between the grid and the vehicle.

## VII. CONCLUSION

The proposed research presents a robust method for tackling the challenges faced in Battery-Wireless Power Transfer (BWPT) systems utilized for Electric Vehicle (EV) charging. The dual-phase shift-regulated PWM technique, in conjunction with a Fuzzy Logic Controller (FLC), provides an enhanced power factor control strategy specifically designed for two-way operations, effectively addressing the shortcomings of conventional power factor control methods. The fuzzy logic controller within the system facilitates real-time adaptive control, enabling smoother modifications to fluctuating grid and load conditions. This significantly improves the overall performance of the BWPT system by dynamically optimizing power transfer, reducing total harmonic distortion (THD), and enhancing power factor correction (PFC) in both Grid-to-Vehicle (G2V) and Vehicle-to-Grid (V2G) modes. A thorough investigation was carried out to assess the system's efficacy, taking into account essential factors such as power factor, bifurcation, THD, and power losses. Simulation results indicate power transfer efficiencies of 94.4% for G2V and 90.1% for V2G modes at a power rating of 3.7 kW and an operating frequency of 85 kHz. The V2G operation utilizing dual-phase shift control and FLC enhances power factor management without significantly impacting the bifurcation factor and THD, while the G2V operation with primary control improves THD and bifurcation performance. This research underscores the significance of advanced control mechanisms, such as fuzzy logic, in the advancement of intelligent and sustainable energy systems. By enabling the seamless integration of EVs into smart grids, the fuzzy logic-enhanced BWPT system increases overall efficiency and guarantees stable, reliable power transfer. Future investigations in BWPT systems are expected to concentrate on scaling the proposed dual-phase shift PWM technology and fuzzy logic control to cater to various power ratings and frequencies. Additionally, the incorporation of Artificial Intelligence (AI) and Machine Learning (ML) techniques could further refine control strategies, enhancing overall system performance.

## REFERENCES

- [1]. M. Venkatesan, N. Rajamanickam, P. Vishnuram, M. Bajaj, V. Blazek, L. Prokop, and S. Misak, "A Review of compensation topologies and control techniques of bidirectional wireless power transfer systems for electric vehicle applications," Energies, vol. 15, no. 20, Oct. 1, 2022, doi: 10.3390/en15207816.
- [2]. Q. He, Q. Luo, K. Ma, P. Sun, and L. Zhou, "Analysis and design of a single-stage bridgeless high-frequency resonant AC/AC converter," IEEE Trans. Power Electron., vol. 34, no. 1, pp. 700–711, Jan. 2019.
- [3]. M.Kim, D.-M.Joo, and B.K.Lee, "Designand control of inductive power transfer system for electric vehicles considering wide variation of output voltage and coupling coefficient," IEEE Trans. Power Electron., vol. 34, no. 2, pp. 1197–1208, Feb. 2019, doi: 10.1109/TPEL.2018.2835161.
- [4]. X. Wang, J. Xu, M. Leng, H. Ma, and S. He, "A hybrid control strategy of LCC-S compensated WPT system for wide output voltage and ZVS range with minimized reactive current," IEEE Trans. Ind. Electron., vol. 68, no. 9, pp. 7908–7920, Sep. 2021, doi: 10.1109/TIE.2020.3013788.



International Journal of Innovative Research in Electrical, Electronics, Instrumentation and Control Engineering
Impact Factor 8.414 

Refereed journal 

Vol. 13, Issue 10, October 2025

#### DOI: 10.17148/IJIREEICE.2025.131012

- [5]. X. Qu, H. Chu, S.-C. Wong, and C. K. Tse, "An IPT battery charger with near unity power factor and load-independent constant output combating design constraints of input voltage and transformer parameters," IEEE Trans. Power Electron., vol. 34, no. 8, pp. 7719–7727, Aug. 2019, doi: 10.1109/TPEL.2018.2881207.
- [6]. X. Liu, N. Jin, X. Yang, K. Hashmi, D. Ma, and H. Tang, "A novel single switch phase controlled wireless power transfer system," Electronics, vol. 7, no. 11, p. 281, Oct. 2018, doi: 10.3390/electronics7110281.
- [7]. V. Shevchenko, O. Husev, R. Strzelecki, B. Pakhaliuk, N. Poliakov, and N. Strzelecka, "Compensation topologies in IPT systems: Standards, requirements, classification, analysis, comparison and application," IEEE Access, vol. 7, pp. 120559–120580, 2019.
- [8]. D. Xu, C. Zhao, and H. Fan, "A PWM plus phase-shift control bidirectional DC–DC converter," IEEE Trans. Power Electron., vol. 19, no. 3, pp. 666–675, May 2004, doi: 10.1109/TPEL.2004.826485. [9]. R. Bosshard, J. W. Kolar, J. Mühlethaler, I. Stevanovic, B. Wunsch, and F. Canales, "Modeling and η–α-Pareto optimization of inductive power transfer coils for electric vehicles," IEEE J. Emerg. Sel. Topics Power Electron., vol. 3, no. 1, pp. 50–64, Mar. 2015, doi: 10.1109/JESTPE.2014.2311302.
- [10]. R. Bosshard and J. W. Kolar, "Inductive power transfer for elec tric vehicle charging: Technical challenges and tradeoffs," IEEE Power Electron. Mag., vol. 3, no. 3, pp. 22–30, Sep. 2016, doi: 10.1109/MPEL.2016.2583839.
- [11]. M. Neath, "Bidirectional inductive power transfer system: Analysis and control," Ph.D. dissertation, Univ. Auckland, Auckland, New Zealand, 2013. [Online].. Available: <a href="http://hdl.handle.net/2292/22756">http://hdl.handle.net/2292/22756</a>